Catalysis Today 170 (2011) 3–12

Contents lists available at ScienceDirect

Catalysis Today

journal homepage: www.elsevier.com/locate/cattod

Ex situ characterization of N_2H_4-, $NaBH_4$- and NH_3BH_3-reduced cobalt catalysts used in $NaBH_4$ hydrolysis

S. Cavaliere[a], J. Hannauer[b], U.B. Demirci[b,*], O. Akdim[b], P. Miele[b]

[a] Institut Charles Gerhardt, Université Montpellier 2, CNRS, UMR 5253, Laboratoire des Agrégats Interfaces et Matériaux pour l'Energie, Place Eugène Bataillon, F-34095 Montpellier Cedex 5, France
[b] Université Lyon 1, CNRS, UMR 5615, Laboratoire des Multimatériaux et Interfaces, 43 boulevard du 11 Novembre 1918, F-69622 Villeurbanne, France

ARTICLE INFO

Article history:
Received 27 September 2010
Received in revised form 4 February 2011
Accepted 15 February 2011
Available online 12 March 2011

Keywords:
Cobalt catalyst
Cobalt chloride reduction
Hydrogen release
Sodium borohydride hydrolysis

ABSTRACT

Sodium borohydride $NaBH_4$-reduced cobalt is a very attractive material in catalyzing $NaBH_4$ hydrolysis, as it is highly reactive and cost-effective. However, the nature of its catalytically active phase is still unknown although it has been mostly suggested as being either cobalt boride such as Co_2B or an alloy Co–B. With the objective to contribute to highlight the real nature of the catalytically active phase, we performed a systematic study focusing on synthesizing different Co catalysts, characterizing them by ICP-AES, N_2 adsorption/desorption, EDS, FTIR, DSC, SEM, TEM and XRD, and testing them in $NaBH_4$ hydrolysis. Herein, it is showed that, to be highly reactive, the Co catalyst has to be reduced by a boron-containing reducing agent such as $NaBH_4$ and ammonia borane NH_3BH_3. Furthermore, it has to be amorphous. None of both features were observed in the case of the hydrazine N_2H_4-reduced cobalt. Hence, it is suggested that the presence of boron is necessary to achieve better reactivity through electronic and geometric effects.

1. Introduction

Sodium borohydride (sodium tetrahydroborate, $NaBH_4$) was first synthesized in the 1940s and was soon showed to be a potential hydrogen carrier, capable of releasing molecular hydrogen H_2 (spontaneously or catalytically) by hydrolysis [1]:

$$NaBH_4\,(aq\,or\,s) + (2+\alpha)H_2O\,(l) \rightarrow NaBO_2{\cdot}\alpha H_2O\,(aq\,or\,s) + 4\,H_2 \quad (1)$$

It has especially attracted great attention in the present decade [2] when, in the early 2000s, Amendola et al.'s pioneer work introduced $NaBH_4$ as being one of the most promising solid state hydrogen storage materials owing to a gravimetric hydrogen density of 10.8 wt% [3]. Since then many research groups focused their efforts on trying to make it suitable for technological applications. In fact, research devoted to both $NaBH_4$ as solid state hydrogen storage material and its hydrolysis can be viewed as mainly focusing on the development of efficient catalysts, with the optimization of the effective gravimetric hydrogen density of the system $NaBH_4$–H_2O and the recycling of sodium metaborate by-products $NaBO_2{\cdot}\alpha H_2O$ back into $NaBH_4$ appear to be secondary topics [4]. The recycling is in fact required for $NaBH_4$ because of the storage irreversibility. Indeed, hydrolysis of $NaBH_4$ is highly exothermic (with $\Delta H < -200\,kJ\,mol^{-1}$); in other words, the reverse reaction is highly endothermic, which makes recycling energy-consuming and thus cost-ineffective [2,4–6]. Although today $NaBH_4$ has no more potential for automotive applications (because of too low effective gravimetric hydrogen densities, inefficient recycling of the by-products and expensiveness) [5], it remains attractive for portable and niche ones [6].

Though hydrolysis of $NaBH_4$ is spontaneous, catalysts are necessary to accelerate H_2 release and to achieve the highest yields. A great number of (homogeneous and/or heterogeneous) catalysts have been considered: acids (liquid/solid), metal complexes, metal salts, metals, metal alloys and supported catalysts [4,7]. Metal-based catalysts have attracted significant research attention and among the different metals (such as Fe, Co, Ni, Cu, Ru, Rh, Pd, Ir and Pt) Co has shown to be highly interesting in terms of both reactivity and cost [1,4,7]. Accordingly, many studies have been conducted on developing such Co catalysts as it can be seen from the literature where they can be split into 2 categories. The first one, which is also the most abundant, is application-oriented whereas the second one has a more fundamental approach as it aims to identify the exact nature of the active phase of Co [4,7]. The present work falls in the latter category.

$NaBH_4$ is a strong reducing agent (redox potential of −1.24 V vs. SHE at pH 14 and −0.48 V at pH 0) and thus has the ability to change (reduce) the surface of any Co-based catalysts. This has been first reported by Schlesinger et al. [1] who observed that $NaBH_4$ rapidly

* Corresponding author. Tel.: +33 04 72 44 84 03; fax: +33 04 72 44 06 18.
E-mail address: Umit.Demirci@univ-lyon1.fr (U.B. Demirci).

0920-5861/$ – see front matter © 2011 Elsevier B.V. All rights reserved.
doi:10.1016/j.cattod.2011.02.016

reduces Co^{2+} (from $CoCl_2$) into a black solid assumed to be cobalt boride Co_2B and suggested that it was the catalytically active phase. However, the nature of the as-formed black solid is still unclear; the black solid would be (i) a cobalt boride (Co_xB indicating an intermetallic compound) or (ii) a cobalt-boron alloy (Co–B, i.e. an alloy of some composition).

Various cobalt borides Co_xB have been suggested to form so far: CoB [8], Co_2B [1], Co_3B [9] and Co_xB [10]. The x value depends on the experimental conditions of synthesis and processes involved in recovering, washing, and drying of the catalyst [11–13]. It is highly interesting to notice that XRD was often used to characterize the Co-based black powder, which showed to be amorphous with at least one broad peak centered at around $2\theta = 45^\circ$. XRD is useful in determining the material crystallinity (i.e. its amorphous state) but it is not really applicable in assigning the chemical nature (e.g. a boride). Be that as it may, the formation of Co_xB was even so proposed.

In contrast, Jeong et al. [14], Fernandes et al. [15] and Wang et al. [16] have reported the formation of a Co–B alloy. For example, Wang et al. [16] observed, by XPS characterizations, that the B 1s binding energy (188.1 eV) was positively shifted of 1.1 eV in relation to the binding energy of B^0 (187.2 eV) while the binding energy of Co^0 shifted negatively by 0.5 eV. Such shifts imply an electron transfer from alloying B to vacant d-orbital of Co^0 in the amorphous Co–B alloy, making B electron-deficient and Co electron-rich and thus Co catalytically more active [17].

There is thus divergence concerning the nature of Co catalyst that activates $NaBH_4$ hydrolysis. This is well illustrated by the following works. Dai et al. [18] and Garron et al. [19] used quite similar experimental conditions to obtain Co catalysts and they nevertheless arrived at different conclusions, which were the formation of Co–B and Co_2B, respectively. Such divergence asks questions. Is Co_xB or Co–B really the catalytically active phase? Might there be a part of subjectivity when one Co compound rather than another one is suggested (from e.g. elemental analysis and/or XRD results)? Might there be any dependence of the experimental conditions and the nature of Co precursor [20] on the formation of Co_xB and Co–B?

Answering the questions above is not at this moment obvious and the present study aims to provide elements of answer in order to better understand the nature and the behavior of the catalytically active Co phase. In this way, $CoCl_2$ was used as catalyst precursor and was reduced with three different reducing agents (hydrazine, sodium borohydride and ammonia borane). $NaBH_4$ is mostly used as reducing agent and our objective in using other reducing agents was to contribute in highlighting the nature of the catalytically active Co phase. For example, it is showed herein that boron is necessary in the catalyst. The obtained Co-based catalysts were characterized by ICP-AES, N_2 adsorption–desorption, DSC, XRD, SEM, EDS, TEM and XPS in fresh and used forms, and were compared in the $NaBH_4$ hydrolysis. The main results are reported and discussed.

2. Experimental

2.1. Materials

Sodium borohydride ($NaBH_4$, 99%, Acros Organics) and ammonia borane (NH_3BH_3, 98%, Aldrich) were used as received and were handled in an argon-filled glove box. Cobalt chloride hexahydrate ($CoCl_2{\cdot}6H_2O$, ≥99%, Sigma–Aldrich), sodium hydroxide (NaOH, ≥98%, Sigma–Aldrich), hydrazine (N_2H_4, 98%, Sigma–Aldrich) and tetrahydrofuran (C_4H_8O, THF, 99%, Sigma–Aldrich) were used as received. All experiments were performed using ultra pure water (Milli-Q grade; resistivity >18 MΩ cm).

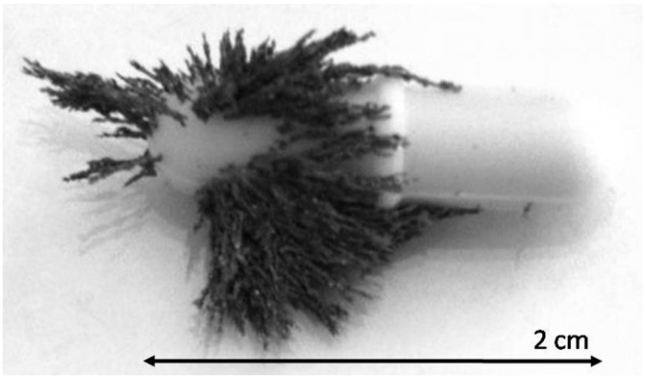

Fig. 1. Picture of CoH_0 on a magnetic stirrer.

2.2. Synthesis of the Co catalysts

In order to prepare the Co-based catalysts (denoted CoX_0); with X referring to the reducing agent used; namely, H as hydrazine, B as sodium borohydride, B′ as ammonia borane; 0 means fresh catalyst; instead of 0, Figs. 1–3 can be used to refer to the catalyst–$NaBH_4$ mixtures, the used catalysts and the annealed CoX_2, respectively), cobalt chloride hexahydrate was reduced with different reducing agents in different conditions. Each of the synthesis was done under Ar atmosphere using Schlenk glassware and the synthesized catalysts were kept and handled in an Ar-filled glove box. $CoCl_2{\cdot}6H_2O$ was also used directly to hydrolyze $NaBH_4$ (denoted as $CoCl_2$_0, $CoCl_2$_1 and $CoCl_2$_2 for fresh), $NaBH_4$-mixed and used precursor.

To synthesize CoH_0, a volume of 20 mL of N_2H_4 was added dropwise into 75 mL of an aqueous solution of $CoCl_2{\cdot}6H_2O$ (0.2 M) at 100 °C under reflux. The mixture was stirred for 3 h. The resulting brilliant grey magnetic powder was rinsed with water until pH 7 and dried under vacuum.

CoB_0 was prepared by chemical reduction, as reported elsewhere [21,22]. Typically, an aqueous solution of $CoCl_2{\cdot}6H_2O$ (0.2 M, 50 mL) was reduced with a NaOH-stabilized (0.1 M) aqueous solution of 1 M $NaBH_4$. The $NaBH_4$ solution was added dropwise while the chloride solution was being kept in an ice-cooled water bath. The mixture was then stirred for 1 h. The as-obtained black powder, which showed to be magnetic, was washed with water until pH 7 and dried under vacuum at room conditions.

Similar experimental conditions to those of CoB_0 in terms of concentrations were used to prepare CoB′_0. Typically, CoB′_0 was synthesized by adding dropwise 50 mL of a mixture of 1 M NH_3BH_3 and 0.1 M NaOH into 50 mL of 0.2 M $CoCl_2{\cdot}6H_2O$ aqueous solution in an ice-cooled bath. The mixture was stirred for 1 h. The as-obtained black magnetic powder was then rinsed with water until pH 7 and dried under vacuum at room conditions.

2.3. Preparation of the $NaBH_4$–CoX_0 mixtures

Hydrolysis was performed with solid $NaBH_4$ that was premixed to CoX_0 prior to any test. This was done according to a procedure reported elsewhere [23]. It was shown that the 'solvent-based method' consisting in dissolving and mixing $NaBH_4$ and $CoCl_2$ together in THF improves the catalyst reactivity in terms of activation time, hydrogen generation rate and total conversion compared to the mechanical mixing of both solids in a mortar. Accordingly, 450 mg of $NaBH_4$ and 110 mg $CoCl_2{\cdot}6H_2O$ or 50 mg CoX_0 (10 wt% (Co)) were transferred in a Schlenk flask sealed with a silicon septum under Ar atmosphere. Then, 50 mL of THF was added. The mixture was stirred for 1 h at room conditions. A needle was let through the silicon septum in order to let any released hydrogen

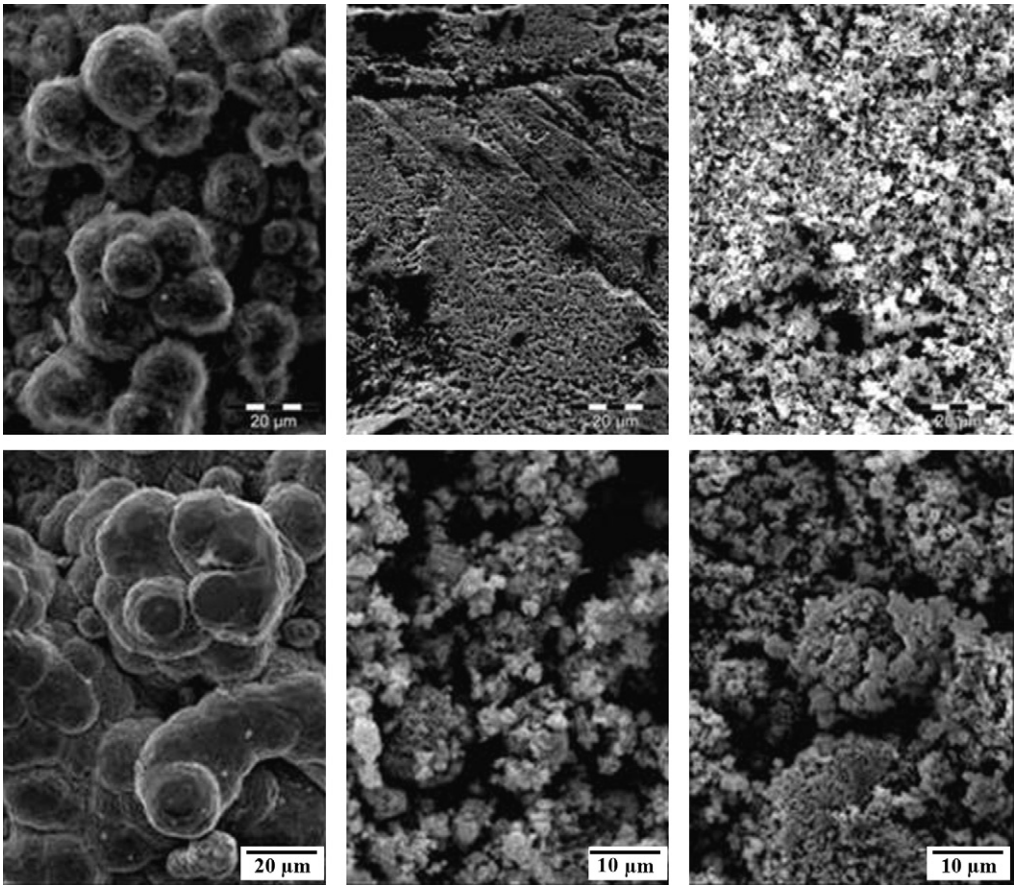

Fig. 2. SEM pictures of CoH_0 (top left), CoB_0 (top middle) and CoB′_0 (top right), and of CoH_2 (bottom left), CoB_2 (bottom middle) and CoB′_2 (bottom right).

leak out. Finally, the solvent was evaporated and the solid mixture dried under vacuum at room temperature. The as-prepared CoX_1 samples were then recovered, milled and kept in the Ar-filled glove box.

2.4. Preparation of CoX_2 and CoX_3

CoX_0, i.e. CoX_1, was used in the hydrolysis of $NaBH_4$ (as described in Section 2.6) and, upon the hydrolysis completion, used CoX_0 was separated from the reaction slurry. Typically, the spent solution was extracted, the catalyst washed with deionized water until pH 7 and then dried under vacuum. All the process was done under Ar atmosphere using Schlenk glassware. In this way, CoX_2 was recovered.

From DSC experiments (see Section 2.5), the annealing temperature of CoX_2 was chosen. It was 600 °C. Accordingly, the CoX_2 materials (100 mg) were annealed at 600 °C (heating rate 10 °C), for 4 h under Ar atmosphere in a furnace. The samples were handled during the whole process under Ar atmosphere, even when transferred from the glove box to the furnace (via an Ar-filled tube,

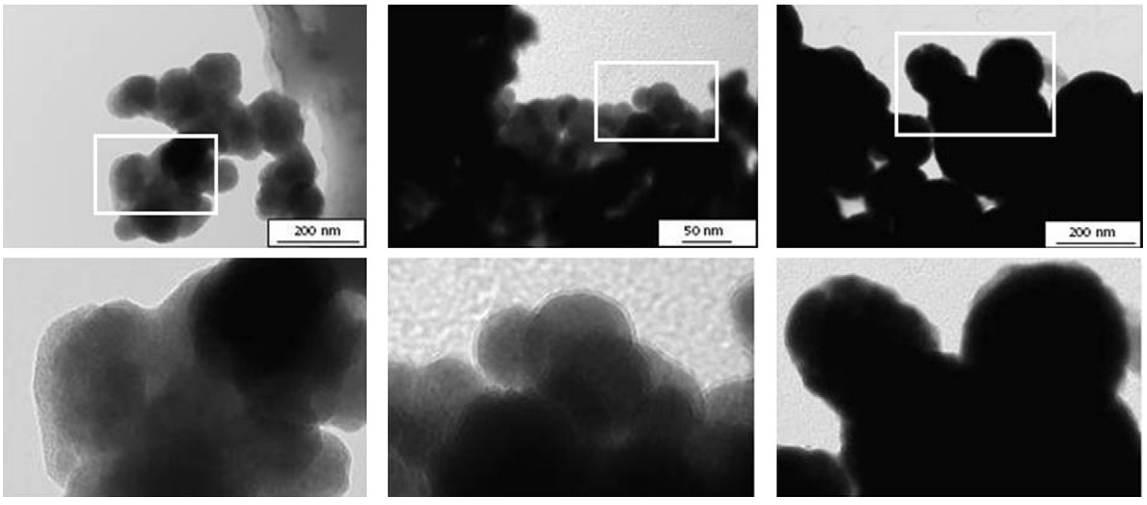

Fig. 3. TEM pictures of CoH_0 (left), CoB_0 (middle) and CoB′_0 (right); the bottom pictures show a magnification (3×) of the particles surface, area indicated by a white-border frame.

sealed in the glove box) and afterwards from the furnace to the glove box.

2.5. Catalysts characterization

Elemental analyses were performed by ICP-AES at the *Service Central d'Analyses* of *CNRS* at Vernaison, France, or at *Service Analyse-Texture* of CNRS IRCELYON at Lyon, France.

Gas nitrogen adsorption/desorption isotherms were measured at 77 K by means of a Micromeritics ASAP 2020 apparatus after outgassing overnight. Specific surface area and average pore width were calculated based on the Brunauer–Emmett–Teller (BET) model.

Structural characterization was performed by X-ray diffraction (XRD; Bruker D5005 powder diffractometer, CuKα radiation (λ = 1.5406 Å). To prevent the material from oxidation and moisture, a Kapton® film was systematically used; in doing so two brad peaks appeared at 2θ of about 22° and 26°.

FTIR analysis was performed by diffuse reflectance Fourier transform infrared spectroscopy (DRIFT-IR, FTIR Nicolet 380).

The catalysts morphology was identified using a Hitachi S800 scanning electron microscope (SEM) equipped with energy-dispersive spectroscopy analysis (EDS) and a JEOL 1200 EXII transmission electron microscope (TEM) operating at 120 kV equipped with a CCD camera SIS Olympus Quemesa (11 million pixels). The samples were suspended in ethanol before deposition onto carbon coated copper grids for TEM analyses. Due to the relevant aggregation of the strongly magnetic CoH_X samples, the simple deposition method was not convenient. Instead, cross-sectional specimens were observed. Prior to perform ultra-thin cross-sections, the samples were embedded in an epoxy resin and allowed to dry at 80 °C for 24 h. Using a Reichert ultramicrotome, 70–90 nm thick microtomies were cut and deposited on 200 square mesh copper grids.

The surface composition of the catalysts was monitored by X-ray photoelectron spectroscopy (XPS) on an ESCALAB 250 (Thermo Electron). The X-ray excitation was provided by a monochromatic Al K_α (1486.6 eV) source. Analyzed surface was 400 μm^2. A constant analyzer energy mode was used for the electron detection (20 eV pass energy). The detection of the emitted photoelectrons was performed perpendicularly to the surface sample. Data quantification was performed on the Advantage program. The background signal was removed using the Shirley method. The surface atomic concentrations were determined from photoelectron peaks areas using the atomic sensitivity factors reported by Scofield. Binding energies (BE) of all core levels were referred to the C–C bond of C1s at 284.8 eV.

In order to determine the annealing temperature to apply to the CoX_2 catalysts to get the CoX_3 materials, differential scanning calorimetry (DSC) measurements were performed with DSC1 (Mettler Toledo) under the following conditions: sample mass 10 mg, aluminum crucible of 100 μl with a pinhole, heating rate of 10 °C min^{-1}, temperature range 25–600 °C, and Ar atmosphere (50 mL min^{-1}). Afterwards, the CoX_2 materials were annealed in greater amounts in a furnace.

2.6. Hydrogen generation measurement

A typical hydrogen generation measurement was performed as follows. In the Ar-filled glove box, CoX_1 was introduced into the reactor consisting of a glass tube (16 mm diameter). The reactor was then sealed with a silicon septum. It was placed in a water bath thermostated at 80 °C. The room temperature was 20 °C. Deionized water (0.5 mL, mol ratio $H_2O/NaBH_4$ equal to 9) was then injected in the tube. The reactor exhaust was connected to a water-filled inverted burette. No stirring was used, except that induced by H_2 evolution. All the measurements were video-recorded. The hydrogen generation rate *r* (also denoted HGR) was determined at 50% of $NaBH_4$ conversion (without taking into account any possible occurring lag phase). The rate *r* may be given either in L(H_2) min^{-1} or in L(H_2) min^{-1} g^{-1} (Co). Each hydrogen generation measurement was carried out twice.

Table 1
Chemical composition of CoX_0 and CoX_2 by ICP-AES.

	Co (wt%)	B (wt%)	$Co_\alpha B_\beta$ [a]
CoH_0	96.2	0[b]	Co
CoB_0	82.8	8.1	$Co_{1.9}B$
CoB′_0	82.0	3.6	$Co_{4.2}B$
$CoCl_2$_0	–	–	–
CoH_2	95.6	0[c]	Co
CoB_2	88.3	2.9	$Co_{5.6}B$
CoB′_2	88.5	3.1	$Co_{5.2}B$
$CoCl_2$_2	79.3	2.3	$Co_{6.3}B$

[a] $Co_\alpha B_\beta$ compound that might be suggested.
[b] <20 ppm.
[c] <100 ppm.

3. Results

3.1. CoX_0

Both CoB_0 and CoB′_0 were powdery black solids. CoH_0 consisted in small brilliant grey needles (Fig. 1); this indicates that a bulk metal was obtained. Care was needed during handling as the material showed strong magnetic properties.

The bulk chemical composition of the CoX_0 samples in terms of B and Co contents was determined by elemental analysis (Table 1). No boron was found in CoH_0 whereas significant amounts were detected for both CoB_0 and CoB′_0. Assuming that the catalysts had a uniform global composition, this would indicate Co, $Co_{1.9}B$ and $Co_{4.2}B$ as CoH_0, CoB_0 and CoB′_0, respectively. The result related to CoB_0 is quite similar to Schlesinger et al.'s, who proposed the formation of Co_2B [1]. Evaluation of the surface chemical composition of CoX_0 was obtained by EDS (Table 2). It confirmed the absence of boron in CoH_0. For both CoB_0 and CoB′_0, the atomic ratio Co/B was lower than that found by elemental analysis. Taking into account the semi-quantitative nature of EDS, this suggests that boron was mostly located onto the surface of the CoB_0/CoB′_0 particles, with the inner layer of the catalysts being richer in Co [24].

The CoX_0 morphology was visualized by SEM. Fig. 2 depicts the surface of the fresh catalysts. The surface of CoH_0 showed stacked big aggregates of 10–20 μm. The surfaces of CoB_0 and CoB′_0 were quite similar; they showed very small particles at a magnification of 20 μm. The catalysts were also analyzed by TEM (Fig. 3). CoH_0 consisted of 40–120 nm nanoparticles that are slightly aggregated, due to the magnetic nature of the material. The particles were covered with a layer that revealed the surface oxidation consistent with the EDS measurements. CoB_0 showed smaller nanoparticles

Table 2
Surface chemical composition of CoX_0 and CoX_2 by EDS.

	Co (wt%)	B (wt%)	$Co_\alpha B_\beta$ [a]
CoH_0	12.7	0	Co
CoB_0	87.2	12.8	$Co_{1.3}B$
CoB′_0	89.7	6.8	$Co_{2.4}B$
$CoCl_2$_0	–	–	–
CoH_2	95.6	0	Co
CoB_2	93.6	5.6	$Co_{3.1}B$
CoB′_2	93.4	5.5	$Co_{3.1}B$
$CoCl_2$_2	90.1	6.4	$Co_{2.6}B$

[a] $Co_\alpha B_\beta$ compound that might be suggested.

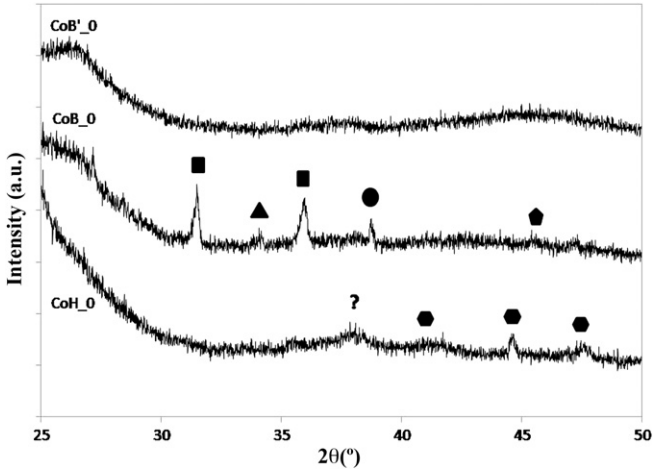

Fig. 4. XRD patterns of CoH_0 (hexagon: hexagonal Co ICDD 00-001-1278;?:CoO ICDD 01-074-2391 or Co_3O_4 ICDD 03-065-3101 or $Co(OH)_2$ ICDD 00-030-0443), CoB_0 (square: NaOH ICDD 00-015-0895; triangle: CoO ICDD 01-075-0419; circle: CoOOH ICDD 01-073-1213; and pentagon: hexagonal Co ICDD 00-001-1277) and CoB′_0.

of 10–60 nm but they were strongly aggregated [19,25,26]. Furthermore, one can see a 2 nm-thick thin layer that covered the nanoparticles. With respect to CoB′_0, it resembled CoB_0 even though the particles were a little bit bigger (100–200 nm) and the outer layer thicker (5–10 nm). The layers may be ascribed to superficial borates [25–27] as well as to cobalt oxide [28].

The crystallinity nature of the surfaces was investigated by XRD (Fig. 4). The patterns indicate the amorphous nature of each CoX_0 even though few small peaks were depicted in the cases of CoH_0 and CoB_0. The XRD pattern of CoH_0 showed peaks at around 2θ 42°, 45° and 48° ascribed to hexagonal Co (ICDD 00-001-1278); a broader peak at 2θ 38° was also observed and probably due to the presence of CoO (ICDD 01-074-2391), Co_3O_4 (ICDD 03-065-3103) or $Co(OH)_2$ (ICDD 00-030-0443). Regarding CoB_0, the two main peaks at 2θ 31° and 36° were ascribed to NaOH (ICDD 00-015-0895); the peaks at 2θ 34°, 39° and 47° were identified as being CoO (ICDD 01-075-0419), CoOOH (ICDD 01-073-1213) and hexagonal Co (ICDD 00-001-1277), respectively. The pattern of CoB′_0 showed two broad peaks at around 2θ 38° and 45°, revealing its amorphous nature. Throughout the literature, such XRD pattern appeared to be an evidence of the formation of either cobalt boride or a cobalt–boron alloy. For example, the reference pattern of Co_2B (ICDD 00-025-0241) shows peaks at 2θ 38° and 45° with relative intensities of 20 and 100%, respectively. Hexagonal Co (ICDD 00-001-1278), CoO (ICDD 01-074-2391) and Co_3O_4 (ICDD 03-065-3103) show peaks of high intensity at 2θ 38 ± 1° and/or 45 ± 1° and our XRD patterns indicate that these compounds may have formed.

The chemical state of the CoX_0 surfaces was studied by XPS. Table 3 shows the binding energy (BE) values of Co 2p3/2, B 1s and O 1s and proposes the likely Co compounds that might have formed [29,30]. The results show that the Co surface sites are mostly in an oxidized state. Consistently with the previous characterizations, the CoH_0 surface appeared to consist of Co, cobalt oxides (e.g. CoO, Co_2O_3 and/or Co_3O_4) and cobalt hydroxide $Co(OH)_2$ in agreement with the O 1s core level spectrum. The Co 2p3/2 BE (778.1 eV) is even very close to that of metal Co (778.0 eV). The XPS results also suggest that CoB_0 is composed of Co, Co oxides and $Co(OH)_2$. The BE 187.7 eV of B 1s is positively shifted of 0.5 eV in relation to the BE of B (187.2 eV) while the Co 2p3/2 BE 777.7 eV is slightly decreased (0.3 eV) compared to the BE of Co (778 eV). Such shifts suggest an electron density transfer from B to vacant d-orbital of Co [17], one plausible reason being strongly adsorbed B-based compounds over adsorbing Co sites. Furthermore, the surface of CoB_0

Table 3
XPS results: Co 2p3/2, B 1s and O 1s binding energies of CoX_0.

	Element	Peak BE (eV)	Atomic %	Likely compounds[a]
CoH_0	Co 2p3/2	778.1	0.8	Co
		780.6	4.3	$Co(OH)_2$, CoO
		782.6	2.0	Co_3O_4
		786.2	2.4	Co_2O_3, $Co(OH)_2$
	O 1s	529.3	3.3	CoO, Co_3O_4
		531.3	36.7	$Co(OH)_2$
		533.2	4.3	H_2O
		535.8	4.0	Adsorbed H_2O/OH
CoB_0	Co 2p3/2	777.7	1.4	Co
		780.2	2.9	CoO, Co_3O_4, $Co(OH)_2$
		782.3	1.3	Co_3O_4, $Co(OH)_2$
		785.7	1.6	Co_2O_3, $Co(OH)_2$
	O 1s	530.5	13.7	Co_2O_3
		531.5	16.9	$Co(OH)_2$
		533.3	4.8	B_2O_3, H_2O
	B 1s	187.7	2.8	B
		191.4	6.2	Boron oxides[b]
CoB′_0	Co 2p3/2	–[c]	–[c]	–[c]
	O 1s	–[c]	–[c]	–[c]
	B 1s	–[c]	–[c]	–[c]

[a] [28,29].
[b] $Na_2B_4O_7$, $Na_3B_3O_6$, BO_2^-: with B 1s BEs of 191.6, 191.7, and 191.8 eV, respectively.
[c] Not determined because of peak fit problems; the spectra showed too wide peaks, maybe due to charge effects.

would have contained borates; the BE (191.4 eV) reported here is quite similar to that of $Na_2B_4O_7$ (191.6 eV), $Na_3B_3O_6$ (191.6 eV) and BO_2^- (191.8 eV). This is consistent with Kim et al.'s work [27], which showed that a film consisting of $Na_2B_4O_7{\cdot}10H_2O$ and boron oxides (B_xO_y, B_2O_3) formed after the catalyst brought into contact the borohydride anions. Concerning CoB′_0, its analysis by XPS was impeded by a problem while attempting to fit the peaks. The high resolution spectra (not reported) systematically displayed wide peaks and led to a high error in the BE of the C–C bond of C1s. Maybe, this might be due charge effects. Despite that limitation, the spectra were tentatively deconvoluted: the peak of Co 2p3/2 showed at least two peaks, with the first having a hypothetical BE of 778.6 ± 0.7 eV (ascribed to Co) and the other(s) being at higher values (ascribed to oxides and hydroxide); the peak of B 1s showed two peaks whose BEs could not be determined; the peak of O 1s appeared to be symmetrical and its deconvolution was discarded.

3.2. CoX_1

The CoX_1 samples were characterized by XRD and IR to verify the presence of crystallized $NaBH_4$. The XRD patterns (not reported) clearly evidenced it. This was also confirmed by IR as the obtained spectra (not reported) showed its fingerprint.

Fig. 5 shows the hydrogen evolution obtained for $CoCl_2$_1, CoH_1, CoB_1 and CoB′_1. In terms of HGRs, the following order was found: $CoCl_2$_0 > CoB′_0 > CoB_0 > CoH_0, with r equal to 268, 41, 25, and 5 mL min^{-1}, respectively. The highest reactivity of the chloride has been already reported [31] and it is known that the in situ formed Co nanoparticles (through the reduction of $CoCl_2$) have an initial high reactivity that decreases when they are recovered, washed and reused (process similar to the ex situ synthesis of the Co nanoparticles). The reactivity loss is generally ascribed to the nanoparticles aggregation during both the hydrolysis and the recovery process [19,28].

The specific surface areas (Table 4) of CoB′_0 and CoB_0 were determined to be 18 and 8 $m^2\ g^{-1}$, respectively. Though higher reactivity is expected with higher specific surface areas, our result is inconsistent with the difference in reactivity previously reported (i.e. CoB′_0 > CoB_0). This is not well understood; accordingly further studies are in progress. Nevertheless, as showed hereafter, XPS

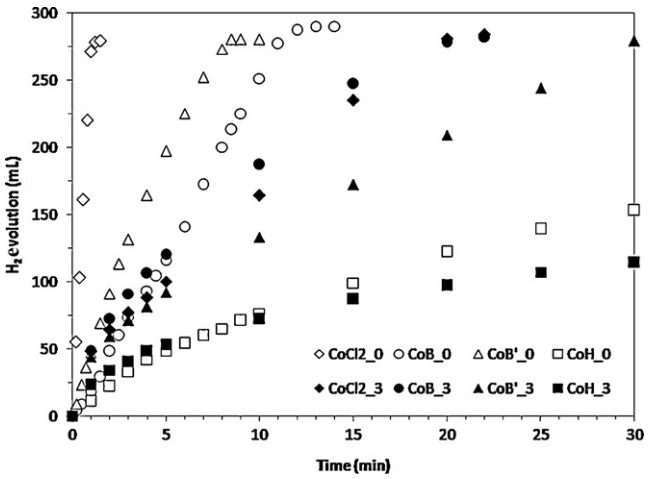

Fig. 5. Hydrogen evolutions obtained for $CoCl_2$_0, CoH_0, CoB_0 and CoB′_0 as well as for $CoCl_2$_3, CoH_3, CoB_3 and CoB′_3.

results would suggest more reactive Co sites (electronic effects). Also, the specific surface area was determined for CoX_2 (recovered, washed until pH 7 and dried under vacuum) and it was found that $CoCl_2$_2 had a slightly higher specific surface area than that of CoB_0. The specific surface area of CoB_2 was slightly lower than CoB_0, due to an aggregation of the Co nanoparticles. Thus, the observations are in favor of a higher reactivity of the precursor of $CoCl_2$_2. Surprisingly, the area of CoB′_2 was slightly increased. The lowest reactivity of CoH_0 can be attributed to the catalyst surface nature as XPS results suggest the presence of lowly reactive oxide and/or hydroxide and to its crystallinity.

3.3. CoX_2

After hydrolysis, CoX_2 was all recovered under Ar atmosphere. CoH_2, CoB_2 and CoB′_2 had the same physical aspect of CoX_0, namely a grey metallic powder. Regarding $CoCl_2$_0, it became magnetic powdery black solid ($CoCl_2$_2). The chemical compositions by ICP-AES and the surface chemical composition by EDS were determined (Tables 1 and 2). Compared to the original materials CoB_0 and CoB′_0, the compositions of CoB_2 and CoB′_2 were modified, the boron content having decreased, suggesting a stoichiometry of $Co_{5.6}B$ and $Co_{5.2}B$, respectively. The composition of $CoCl_2$_2 was quite similar to that of CoB_2. The main observation is that only traces of boron (<100 ppm) were found for CoH_2.

Table 4
Specific surface area (S_{BET}), adsorption average pore with (AAPW) and pore volume (V_{POR}) of CoX_0 and CoX_2 catalysts.

	S_{BET} ($m^2\ g^{-1}$)	AAPW (Å)	V_{POR} ($cm^3\ g^{-1}$)
CoH_0	–	–	–
CoB_0	18	235	0.104
CoB′_0	8	97	0.019
$CoCl_2$_0	–	–	–
CoH_2	–	–	–
CoB_2	15	371	0.141
CoB′_2	10	194	0.050
$CoCl_2$_2	20	267	0.132

The SEM images of CoX_2 are given in Fig. 2. There was apparently no change in the surface morphology of CoH_2, CoB_2 and CoB′_2 compared to CoH_0, CoB_0 and CoB′_0. The morphology of $CoCl_2$_2 (not reported) was very similar to that of both CoB_0 and CoB′_0. By TEM (Fig. 6), it can be observed that the morphology of the Co-based catalysts had changed after hydrolysis. The CoH_2 showed the presence of spherical nanoparticles of various sizes from few tens to hundreds nanometers. Their surface was covered by an irregular layer [25,26] and, in the case of CoB_2, the thin layer was more irregular than that on CoB_0. For CoB′_0, the nanoparticles' aggregation was more extensive and the layer was irregular. The contact of the CoB′_0 nanoparticles with $NaBH_4$ had manifestly led to a change of its surface but the outer layer was still present.

The CoX_2 materials were analyzed by XRD (Fig. 7). With respect to CoH_2, peaks at around 2θ 42°, 45° and 48° were detected. They can be ascribed to hexagonal Co (ICDD 00-001-1278). For both CoB_2 and CoB′_2, similarly to CoB_0 and CoB′_0, two broad peaks at around 2θ 36° and 45° indicative of their amorphous nature are displayed. $CoCl_2$_2 pattern shows two broad peaks at around 2θ 36° and 45° (consistently with CoB_2 and CoB′_2) and small sharp peaks at around 2θ 42°, 45° and 48° ascribed to hexagonal Co (ICDD 00-001-1278).

The surface of the CoX_2 catalysts was analyzed by XPS (Table 5). The surface of CoH_2 was oxidized, with no Co being detected, which may be due to the washing process. Therefore, CoH_2 consisted of Co oxides and $Co(OH)_2$ as no boron was found. CoB_2

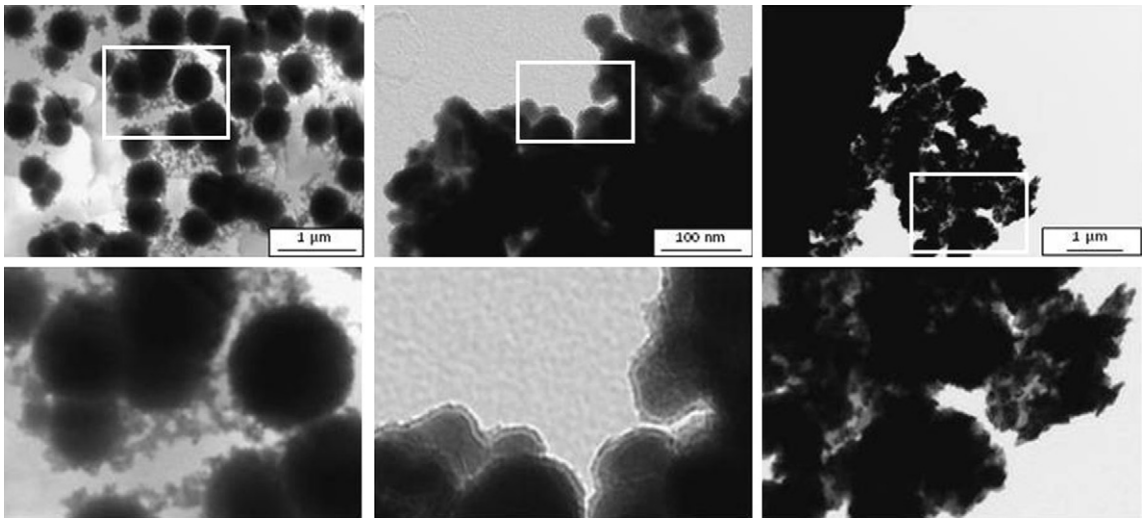

Fig. 6. TEM pictures of CoH_2 (left), CoB_2 (middle) and CoB′_2 (right); the bottom pictures show a magnification (3×) of the particles surface, area indicated by a white-border frame.

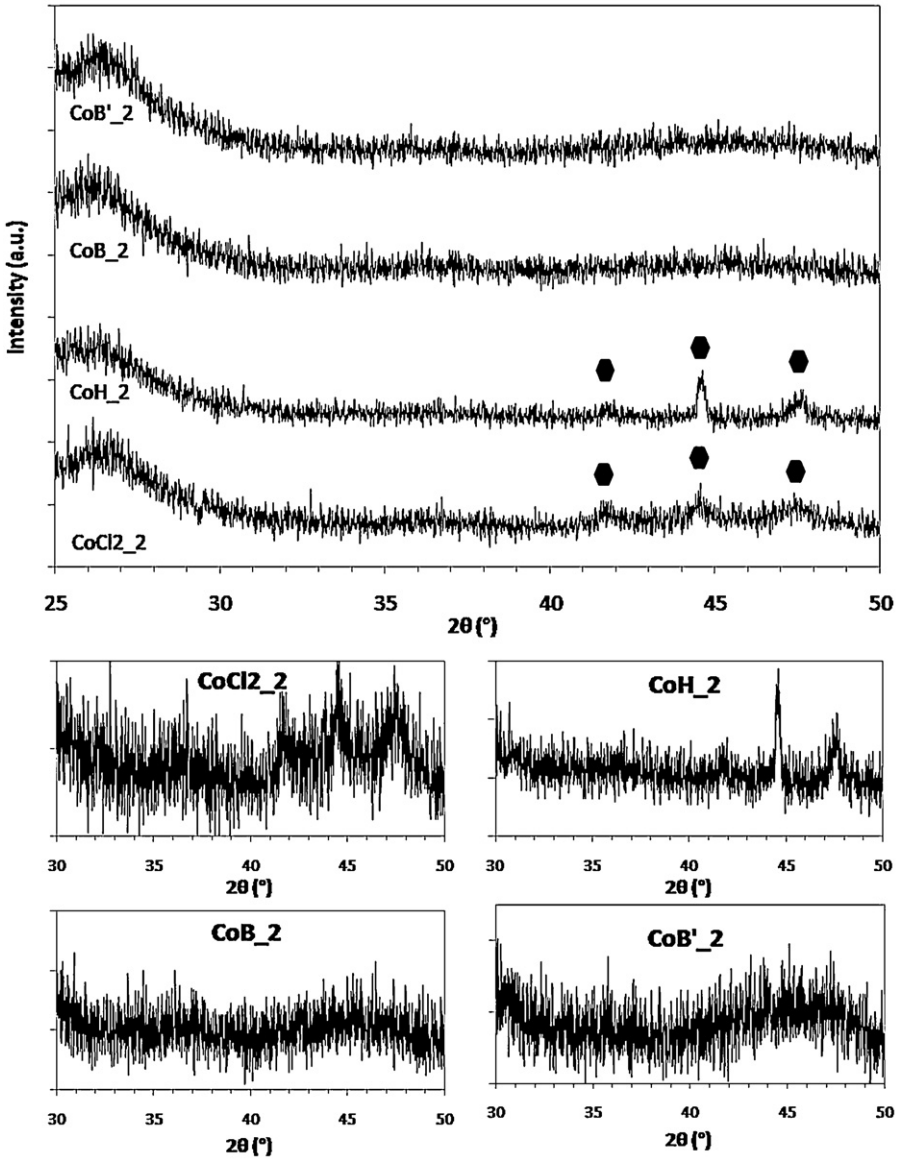

Fig. 7. XRD patterns of $CoCl_2$_2, CoH_2, CoB_2 and CoB′_2 (magnifications over 2θ 30–50° are given to better show the broad peaks at around 36° and 45°).

contained Co, Co oxides and $Co(OH)_2$ but the content of Co decreased in relation to that in CoB_0. Its surface oxidation degree increased. An electron transfer from B to Co is as likely as in CoB_0. Further, the surface contained borate-based compounds. These observations are consistent with those made for CoB_0. With respect to CoB′_2, it also consisted of Co oxides and $Co(OH)_2$, with a small content of Co. Compared to Co (BE of 778.0 eV), a negative shift of 0.8 eV is remarkable for the Co 2p2/3 BE 777.2 eV whereas no shift is observed for the B 1s BE 187.0 eV. A BE of 777.2 eV has been attributed to metallic Co elsewhere [32]. Such Co should be more reactive owing to an increased electron-donor ability toward electron-deficient boron in BH_4^-. This might explain why CoB′_0 was more reactive than CoB_0 (Fig. 5). Moreover, the CoB′_2 surface contained borate-based compounds. With respect to $CoCl_2$_2, the situation was similar to that of CoB_0 or even to CoB_2. Its surface was composed of Co, Co oxides and $Co(OH)_2$. The B 1s BEs showed significant positive shifts in relation to B (+1.1 eV) and the shift was higher to that measured for the other Co catalysts. The presence of surface borates such as BO_2^- and B_2O_3 suggests the occurrence of an electron transfer from B to neighboring O [22].

3.4. CoX_3

Glavee et al. [13] have reported that annealing (at 500 °C for 2 h under Ar) the Co nanoparticles obtained through reduction of $CoCl_2$ by $NaBH_4$ leads to the formation of the cobalt boride Co_2B. A similar procedure was used in some other studies to support that the nature of the Co catalyst is a boride [9,12,33], the annealed material being characterized by XRD. Such an approach was also applied in our work.

The annealing temperature was first determined from DSC experiments (Fig. 8), which showed the CoX_2 materials behave differently under heating. For CoH_2, a small exothermic peak at around 350 °C was observed. CoB_2 showed an exothermic peak at 455 °C (onset temperature at 445 °C) which enthalpy is of 7.2 kJ mol^{-1} (Co). Another one at around 350 °C seemed to occur but it overlapped the decreasing baseline. For CoB′_2, two exothermic peaks at 340 and 460 °C are depicted (onset temperatures of about 327 and 454 °C); the enthalpies are calculated as being 1.3 and 2.9 kJ mol^{-1} (Co). Three exothermic processes were observed in the case of $CoCl_2$_2: the first one at 350 °C (onset temperature at 328 °C), the second one at 365 °C (onset temperature at 358 °C) and

Table 5
XPS results: Co 2p3/2, B 1s and O 1s binding energies of CoX_2.

	Element	Peak BE (eV)	Atomic %	Likely compounds[a]
CoH_2	Co 2p3/2	780.5	0.5	$Co(OH)_2$, CoO
		782.5	0.4	Co_3O_4
		785.9	0.4	Co_2O_3, $Co(OH)_2$
	O 1s	530.6	2.9	Co_2O_3
		531.8	14.5	$Co(OH)_2$
		533.2	10.0	H_2O
		535.5	4.9	Adsorbed H_2O/OH
CoB_2	Co 2p3/2	777.6	0.3	Co
		779.6	2.1	$Co(OH)_2$, Co_3O_4, Co_2O_3
		781.5	1.1	$Co(OH)_2$
		785.6	0.8	Co_2O_3, $Co(OH)_2$
		788.7	0.1	Co_2O_3, $Co(OH)_2$
	O 1s	529.3	4.4	CoO, Co_3O_4
		530.6	10.7	Co_2O_3
		531.8	11.0	$Co(OH)_2$
		533.3	6.5	B_2O_3, H_2O
	B 1s	187.5	1.0	B
		191.2	3.8	$Na_2B_4O_7$, $Na_3B_3O_6$
CoB′_2	Co 2p3/2	777.2	0.6	Co
		780.4	3.9	$Co(OH)_2$, CoO
		782.2	2.2	Co_3O_4
		785.8	1.8	Co_2O_3, $Co(OH)_2$
	O 1s	529.9	Traces	Co_3O_4, $Co(OH)_2$
		530.6	21.1	Co_2O_3
		531.8	18.8	$Co(OH)_2$
		533.0	7.7	B_2O_3, H_2O
	B 1s	187.0	1.1	B
		191.5	7.2	$Na_2B_4O_7$, $Na_3B_3O_6$, BO_2^-
$CoCl_2$_2	Co 2p3/2	777.8	0.3	Co
		780.2	3.7	$Co(OH)_2$, CoO
		782.1	2.4	Co_3O_4
		785.9	2.1	Co_2O_3, $Co(OH)_2$
		789.2	0.2	Co_2O_3, $Co(OH)_2$
	O 1s	529.1	Traces	CoO, Co_3O_4
		530.0	10.0	Co_2O_3
		531.5	21.7	$Co(OH)_2$
		533.2	10.4	B_2O_3, H_2O
	B 1s	188.1	0.5	B
		192.0	5.5	Boron oxides[b]

[a] [28,29].
[b] BO, BO_2^-, B_2O_3, $Na_2B_4O_7$, $Na_3B_3O_6$, $Na_2B_4O_7{\cdot}10H_2O$ with B 1s BEs of 192.0, 191.8, 192.0, 191.6, 191.7, and 192.2, respectively.

the third one at 470 °C (onset temperature at 448 °C). The enthalpies are 3.4, 0.4 and 6.1 kJ mol^{-1} (Co), respectively. Accordingly, the temperature 600 °C was chosen for the annealing of CoX_2. The CoX_3 was obtained.

By XRD (Fig. 9), hexagonal (ICDD 00-001-1278) and cubic (00-089-4307) Co were identified for all of the samples. Both phases

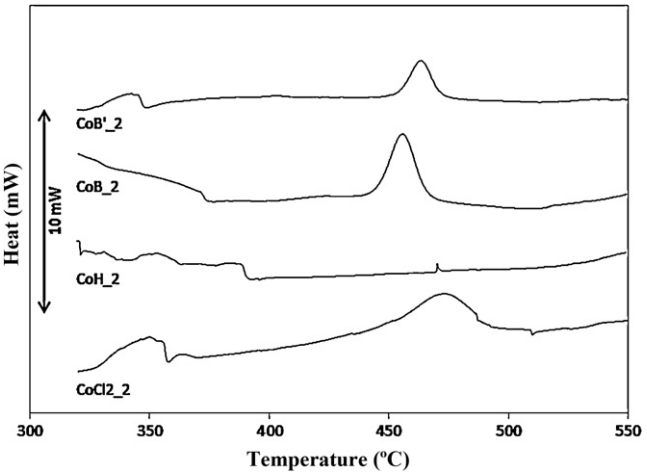

Fig. 8. DSC on $CoCl_2$_2, CoH_2, CoB_2 and CoB′_2.

can coexist at room temperature [34] and even at temperatures above 500 °C [19]. Nevertheless, the hexagonal structure is favored at low temperatures whereas the cubic one is thermodynamically preferred above 450 °C [34]. Wu et al. [33] reported the formation of cubic Co at 300 °C. Accordingly, the exothermic reaction starting at around 330 °C (Fig. 8) may be due to the crystallization of amorphous Co into cubic Co. No other compounds were found for both CoH_3 and $CoCl_2$_3. The XRD patterns of CoB_3 and CoB′_3 show peaks attributed to Co_2B (ICDD 00-025-0241). This might be ascribed to a crystallization of an amorphous Co–B surface compound. Accordingly, the second exothermic peak in DSC (Fig. 8) might be ascribed to such crystallization [35]. Lu et al. [12] also showed the formation of both Co and Co_2B through annealing of $NaBH_4$-reduced $CoCl_2$ at 500 °C. Interestingly, the broad peak at 2θ 45° is still slightly visible on the patterns of CoB_3, CoB′_3 and $CoCl_2$_3; the broad peak at 2θ 36° is also visible for CoB′_2. A part of these catalysts remained amorphous, the calcination temperature being too low for the complete conversion. It is noteworthy that neat crystalline cobalt borides (CoB and Co_2B) form at temperature above 1000 °C [36].

For CoX_3, the H_2 evolutions are given in Fig. 5. The HGR values were determined to be: CoB_3 ~ $CoCl_2$_3 > CoB′_3 > CoH_3, the rates being 19, 17, 12 and 4 mL(H_2) min^{-1}. Annealing has a detrimental effect on the initial reactivity of CoX_0. The negative effect varies from one CoX_3 to the other. It is significant in the case of $CoCl_2$_3, confirming that the in situ formed black solid is much more reactive. With respect to CoB_3 and CoB′_3, the catalytic activity was decreased. This may be attributed to the partial crystallization into hexagonal and cubic Co, and Co_2B. In the presence of CoH_3, the H_2 evolution is slightly decreased compared to that of CoH_3. This is may be due to the formation of cubic Co. Once more this demonstrates that amorphous materials offer a distorted structure leading to high catalytic abilities in $NaBH_4$ hydrolysis. The fact that annealing at 600 °C resulted in sintering is unlikely on the basis of the present characterization data. This might also explain the deteriorated catalytic activity of CoX_3; namely, the bigger the crystallites, the lower the specific surface area, the less active the CoX_3. However, catalyst sintering is a complex process that occurs according to a coalescence and/or Ostwald ripening mechanism, and, if it occurs in our experimental conditions, it has to be studied through a systematic work [37], which is beyond the scope of the present paper. More works are in progress to better understand this phenomenon.

To summarize, the processes involved in recovering, washing, drying and/or annealing are detrimental to the catalysts reactivity, with the Co nanoparticles surface changing.

4. Discussion

The reactivity of the Co catalysts depends on the nature of the reducing agent and on the synthesis approach (i.e. ex situ or in situ). For example, the ex situ NH_3BH_3-reduced Co-based black solid is more active than the ex situ $NaBH_4$-reduced one; this may be due to electronic effects, with the Co sites in the former catalyst being more electron-rich than those on the latter. Another example is that the in situ $NaBH_4$-reduced Co-based catalyst is much more reactive than the ex situ one. This suggests that their respective surfaces are different, with the recovery process of the latter catalyst changing it. Indeed, it was observed that the waste waters of the 2nd to 4th washings had systematically basic pH and this might be taken as an evidence of the borates present on the nanoparticles surface. Furthermore, the partial oxidation of the ex situ formed Co particles during the washing process may also explain such a difference. It is noteworthy that this also suggests that the presence of boron-based compounds does not prevent the Co surface from oxidation.

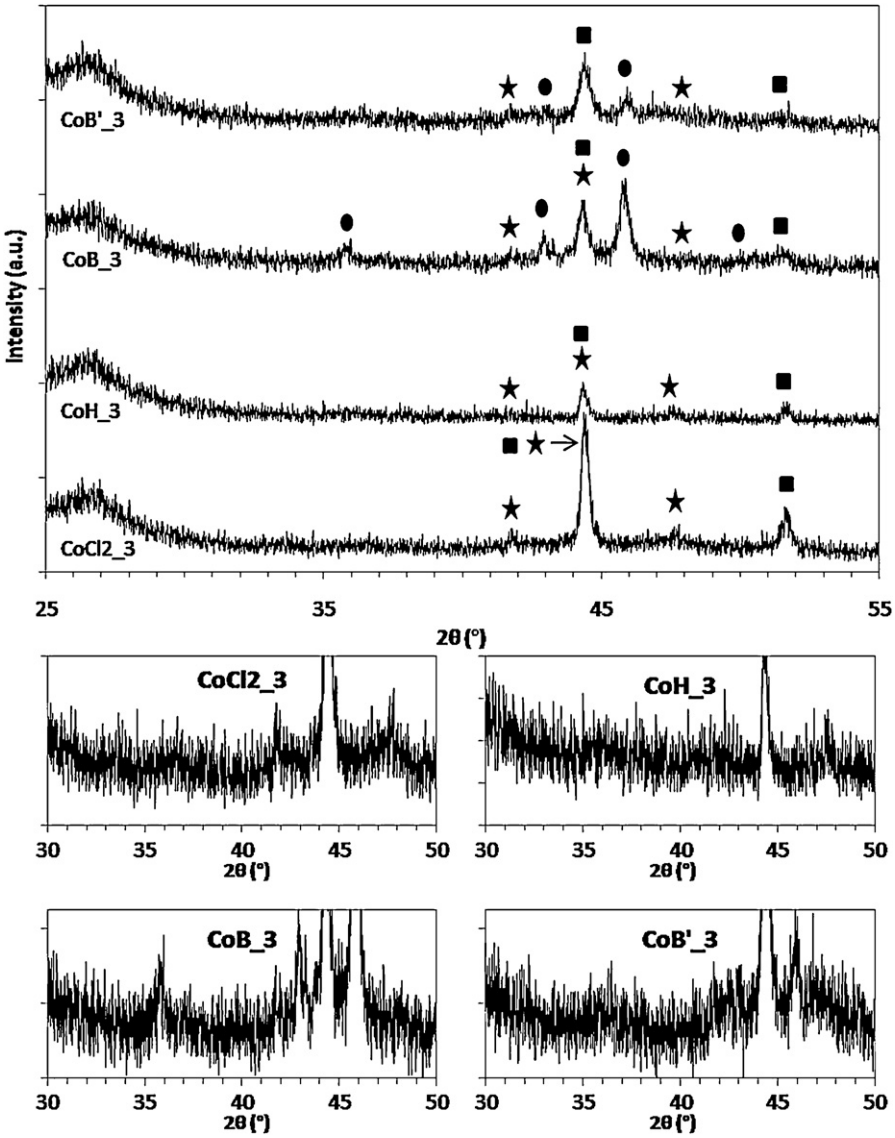

Fig. 9. XRD patterns of $CoCl_2$_3, CoH_3, CoB_3 and CoB′_3; star for hexagonal Co (ICDD 00-001-1278), square for cubic Co (ICDD 01-089-4307) and circle for cobalt boride Co_2B (ICDD 00-025-0241) (magnifications over 2θ 30–50° are given to better show the broad peaks at around 36° and 45°).

The (thorough) washing with water of the Co catalysts, even though neutral pH was systematically met, does not permit to eliminate all of the formed borates [25,27]. Furthermore, the particles suffer from aggregation, which is due to superficial borates that form borate bridges [19,25,26]. This implies that the borates are adsorbed over the Co particles surface. For the ex situ prepared Co catalysts, such agglomerated nanoparticles were used to hydrolyze $NaBH_4$. It is here important to cite Kim et al.'s work [27], as they were the first and only authors to have reported that a film formed over the surface of a Ni catalyst. The film was not removed by washing and was strongly adsorbed. Subsequent analysis found that it consisted of $Na_2B_4O_7{\cdot}10H_2O$, unidentified B_xO_y and B_2O_3. These observations are consistent with our experimental data.

The high activities of the $NaBH_4$- and NH_3BH_3-reduced Co catalysts can also be attributed to their amorphous state. Compared to (partly or totally) crystalline Co compounds, the amorphous equivalents have a much distorted structure and thus more catalytic active sites [38,39].

The N_2H_4-reduced Co catalyst, which may be seen as a reference material to better understand the behavior of the other catalysts, is much less reactive than the other ones. This is due to several reasons such as geometric effects (e.g. higher particle size), crystalline structure and subsequent low reactivity of hexagonal Co, presence of cobalt oxides and hydroxide known to be lowly reactive, and absence of superficial boron/borates.

Taking into consideration all of the observations reported here, we believe that the most important feature is the necessity of boron (in the form of boron and/or borates) in the catalyst for its better reactivity. This has two effects. The first one is to modify the electron density of Co, which makes it more efficient in activating the hydrides of BH_4^- (further studies are in progress to identify the exact nature of the Co sites). Such activated hydrides will then react more easily with protons from adsorbed water in accordance with the bimolecular Langmuir–Hinshelwood mechanism [40]. The second effect is that amorphous cobalt catalysts are formed in its presence, which leads to more catalytic active sites than in crystalline ones. Any crystallization (N_2H_4-reduced Co catalyst or annealing) leads to reactivity deterioration. It is noteworthy that B remains on the Co catalyst surface only when it is provided through the reducing agent; it does not bond to surface Co sites of N_2H_4-reduced during hydrolysis. Besides, the present study asks the following question: would there be Co–O–B interac-

tions between Co and strongly adsorbed surface borates? Specific studies are in progress.

5. Conclusion and challenges

The Co^{2+} cations from $CoCl_2$ reduce when they are in contact with hydrazine, sodium borohydride or ammonia borane. A black solid consisting of nanoparticles is obtained with the boron-based reducing agents whereas a grey bulk metal forms in the presence of the boron-free compound. All of these materials can be used as catalyst in the $NaBH_4$ hydrolysis but they do not show the same reactivity. The three catalysts have been the topic of the present article. They were synthesized, tested in the $NaBH_4$ hydrolysis and characterized by various techniques such as ICP-AES, N_2 adsorption/desorption, EDS, FTIR, DSC, SEM, TEM, and XRD. The main objectives were to highlight the reactivity difference and to attempt to identify the catalytically active phase of the $NaBH_4$- or NH_3BH_3-reduced nanoparticles.

The $NaBH_4$- or NH_3BH_3-reduced Co catalysts showed to be highly active toward the $NaBH_4$ hydrolysis and this has been ascribed to several factors such as the presence of B (as element and/or borates) at the Co nanoparticles surface and the amorphous nature of the catalysts. In contrast, the N_2H_4-reduced Co particles showed to be much less reactive because of their crystalline structure, the presence of surface Co oxides and hydroxide, and the absence of B. In fact, boron is necessary in the catalyst for its better reactivity. It has an electronic effect as it electron-enriches Co, which makes it more efficient in hydrolyzing the borohydride anions. It also has an effect on its crystallization, which is in fact hindered; thus, it favors amorphous materials; this is important as the amorphous state leads to higher catalytic reactivity owing to more distorted structure and subsequently more catalytic sites.

Throughout the literature devoted to $NaBH_4$ hydrolysis, it is mostly reported that the catalytically phase is either a cobalt boride such as Co_2B or an alloy Co–B. To get Co_2B in our experimental conditions, an annealing at 600 °C for 4 h was needed. Furthermore, the characterization data, especially those from XPS, does not support its formation in room conditions. Be that as it may, the present study is a step forward in highlighting the nature of the catalytically active Co phase but there remain several challenges. For example, which is the catalytically active Co phase? A boride Co_xB, an alloy Co–B or any other Co compound [41]? It is obvious that the surface of the catalysts changes and this is problematic since it reveals durability issues. Borates can be found on the catalyst surface. What is(are) their role(s)? May they positively affect the catalyst reactivity given that it has often been claimed that they only act as poisons? Studies are in progress, the objective being to provide elements to answer the questions while addressing the characterization issues. In fact, it seems that the greatest challenge is the in situ characterization (during synthesis as well as hydrolysis) of such Co catalysts [41].

Acknowledgements

We gratefully acknowledge Mr. Franck Godiard of Service Commun de Microscopie Electronique of University of Montpellier 2 for the TEM characterizations, Mrs. Valérie Flaud of Plateforme d'Analyse et de Caractérisation of University of Montpellier 2 for the XPS analysis, Mr. Yannig Nedellec of the AIME-ICGM of University of Montpellier 2 for the fabrication of cross-sectional TEM specimens, Mr. François Toche of the LMI of University Lyon 1 for the DSC experiments, Mr. Samuel Bernard of the LMI of University Lyon 1 for the heat treatments, Mr. Vincent Salles of the LMI of University Lyon 1 for some SEM imaging and the Centre Technologique des Microstructures of University Lyon 1 for the access to the SEM apparatus.

References

[1] H.I. Schlesinger, H.C. Brown, A.E. Finholt, J.R. Gilbreath, H.R. Hoekstra, E.K. Hyde, J. Am. Chem. Soc. 75 (1953) 215–219.
[2] U.B. Demirci, P. Miele, C. R. Chim. 12 (2009) 943–950.
[3] S.C. Amendola, S.L. Sharp-Goldman, M.S. Janjua, N.C. Spencer, M.T. Kelly, P.J. Petillo, M. Binder, Int. J. Hydrogen Energy 25 (2000) 969–975.
[4] U.B. Demirci, O. Akdim, J. Andrieux, J. Hannauer, R. Chamoun, P. Miele, Fuel Cells 10 (2010) 335–350.
[5] U.S. Department of Energy Hydrogen Program, Independent review. Go/no-go recommendation for sodium borohydride for on-board vehicular hydrogen storage. NREL/MP-150-42220, November 2007. Available from: http://www.hydrogen.energy.gov/.
[6] U.B. Demirci, P. Miele, Energy Environ. Sci. 2 (2009) 627–637.
[7] B.H. Liu, Z.P. Li, J. Power Sources 187 (2009) 527–534.
[8] Y. Chen, H. Kim, Energy 35 (2009) 960–963.
[9] J.C. Walter, A. Zurawski, D. Montgomery, M. Thornburg, S. Revankar, J. Power Sources 179 (2008) 335–339.
[10] O.V. Komova, V.I. Simagina, O.V. Netskina, D.G. Kellerman, A.V. Ishchenko, N.A. Rudina, Catal. Today 138 (2008) 260–265.
[11] S. Linderoth, S. Mørup, J. Appl. Phys. 69 (1991) 5256–5267.
[12] J. Lu, D.B. Dreisinger, W.C. Cooper, Hydrometallurgy 45 (1997) 305–322.
[13] G.N. Glavee, K.J. Klabunde, C.M. Sorensen, G.C. Hadjipanayis, Langmuir 9 (1993) 162–169.
[14] S.U. Jeong, R.K. Kim, E.A. Cho, H.J. Kim, S.W. Nam, I.H. Oh, S.A. Hong, S.H. Kim, J. Power Sources 144 (2005) 129–134.
[15] R. Fernandes, N. Patel, A. Miotello, M. Filippi, J. Mol. Catal. A 298 (2009) 1–6.
[16] Y.P. Wang, Y.J. Wang, Q.L. Ren, L. Li, L.F. Jiao, D.W. Song, G. Liu, Y. Han, H.T. Yuan, Fuel Cells 10 (2010) 132–138.
[17] N. Patel, R. Fernandes, G. Guella, A. Miotello, Appl. Catal. B 95 (2010) 137–145.
[18] H.B. Dai, Y. Liang, P. Wang, H.M. Cheng, J. Power Sources 177 (2008) 17–23.
[19] A. Garron, D. Swierczynski, S. Bennici, A. Auroux, Int. J. Hydrogen Energy 34 (2009) 1185–1199.
[20] P. Krishnan, S. Advani, A.K. Prasad, Int. J. Hydrogen Energy 33 (2008) 7095–7102.
[21] H. Li, H. Li, M. Wang, Appl. Catal. A 207 (2001) 129–137.
[22] P. Kukula, V. Gabova, K. Koprivova, P. Trtik, Catal. Today 121 (2007) 27–38.
[23] O. Akdim, U.B. Demirci, P. Miele, Int. J. Hydrogen Energy 34 (2009) 9444–9449.
[24] C.H. Liu, B.H. Chen, C.L. Hsueh, J.R. Ku, F. Tsau, K.J. Hwang, Appl. Catal. B 91 (2009) 368–379.
[25] A. Corrias, G. Ennas, A. Musinu, G. Marongiu, G. Paschina, Chem. Mater. 5 (1993) 1722–1726.
[26] V.S. Khain, Russ. J. Inorg. Chem. 28 (1983) 1410–1413.
[27] J.H. Kim, K.T. Kim, M. Kang, H.S. Kim, M.S. Song, Y.J. Lee, P.S. Lee, P.S. Lee, J.Y. Lee, J. Alloys Compd. 379 (2004) 222–227.
[28] J. Andrieux, D. Swierczynski, L. Laversenne, A. Garron, S. Bennici, C. Goutaudier, P. Miele, A. Auroux, B. Bonnetot, Int. J. Hydrogen Energy 34 (2008) 938–951.
[29] La Surface XPS Database. Available from: http://www.lasurface.com/database/elementxps.php (and references therein).
[30] NIST XPS Database. Available from: http://srdata.nist.gov/xps/Default.aspx (and references therein).
[31] O. Akdim, U.B. Demirci, D. Muller, P. Miele, Int. J. Hydrogen Energy 34 (2009) 2631–2637.
[32] K. Guse, H. Papp, Fresenius J. Anal. Chem. 346 (1993) 84–91.
[33] C. Wu, F. Wu, Y. Bai, B. Yi, H. Zhang, Mater. Lett. 59 (2005) 1748–1751.
[34] D.P. Dinega, M.G. Bawendi, Angew. Chem. Int. Ed. 38 (1999) 1788–1791.
[35] H. Li, Y. Wu, H. Luo, M. Wang, Y. Xu, J. Catal. 214 (2003) 15–25.
[36] S. Sato, O.J. Kleppa, Metall. Mater. Trans. B 13 (1982) 251–257.
[37] M. Bechelany, X. Maeder, J. Riesterer, J. Hankache, D. Lerose, S. Christiansen, J. Michler, L. Philippe, Cryst. Growth Des. 10 (2010) 587–596.
[38] J.M. Yan, X.B. Zhang, S. Han, H. Shioyama, Q. Xu, Angew. Chem. Int. Ed. 47 (2008) 2287–2289.
[39] J.M. Yan, X.B. Zhang, H. Shioyama, Q. Xu, J. Power Sources 195 (2010) 1091–1094.
[40] J. Hannauer, U.B. Demirci, G. Pastor, C. Geantet, J.M. Herrmann, P. Miele, Energy Environ. Sci. 3 (2010) 1796–1803.
[41] U.B. Demirci, P. Miele, Phys. Chem. Chem. Phys. 12 (2010) 14651–14665.